DRAWBAR-PULL CONTROL SYSTEM OF A FLEXIBLE TRACKED VEHICLE ON WEAK TERRAIN

Tatsuro MURO, Prof. Department of Ocean Engineering
Faculty of Engineering, Ehime University

3 Bunkyo-cho, Matsuyama, Japan

ABSTRACT

To establish a drawbar-pull control system to obtain a maximum productivity of a flexible tracked vehicle i.e. a bulldozer running on a super weak marine sediment, the traffic performance of vehicle could be clarified by use of a micro-computer in robotics for construction from the initial information of terrain properties and vehicle dimensions. The optimum drawbar-pull at an optimum slip ratio in dozing operation of an actual large bulldozer running on a self-consolidated kaolinite clay sediment could be determined from the relation between driving force, drawbar-pull, sinkage, trim angle and slip ratio. And also, the tractive performance at braking state i.e. the relations between braking force, effective braking force, sinkage and slip ratio could be presented.

1. Introduction

As an underwater vehicle running on a super weak marine sediment, it should have flexible rubber tracks and larger front and rear wheel in order to accomodate rubber tires of sufficient durability and to provide enough suspension. As the terrain properties, cohesion, angle of internal friction, modulus of shear deformation to calculate the thrust of vehicle, and pressure sinkage curve at rest and relations between slip sinkage, contact pressure and amount of slippage to calculate the locomotion resistance could be estimated by use of input data at several slip ratios from some sensors which could measure the sinkage of rear sprocket at initial and slippage state, the trim angle and the torque.

2. Flexible tracked vehicle

Fig.1 shows a part of the flexible rubber track belt, of which road wheel spacing R_p is 100cm and grouser pitch G_p is 23cm. For flexible tracks, the pressure distribution along the track belt becomes nonuniform. The magnitude of peak pressure under the road wheels depends not only on the number of road wheels and the track tension but also on the soil properties[1].

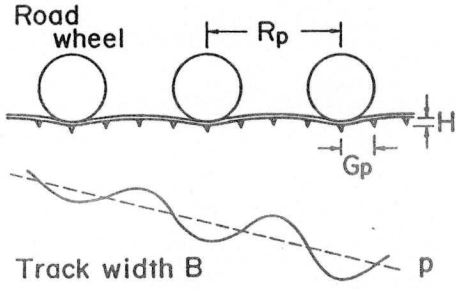

Fig.1 Pressure distribution alog flexible rubber track belt.

Here, assuming that the peak pressure becomes to be 1.2 times as large as the contact pressure acting on a rigid track belt, the multipeak sinusoidal pressure distribution described in Eq.(1) is supposed to act under the flexible tracks.

$$p = \{ p_f + (p_r - p_f) \frac{X}{D} \} \{ 1 + \frac{1}{5} \cos 2\pi n \frac{X}{D}) \} \qquad (1)$$

where p is the contact pressure at the distance X from the frontidler, p_f and p_r is the pressure under the bottom of front and rear wheel respectively, D is the contact length of track belt, and n is the number

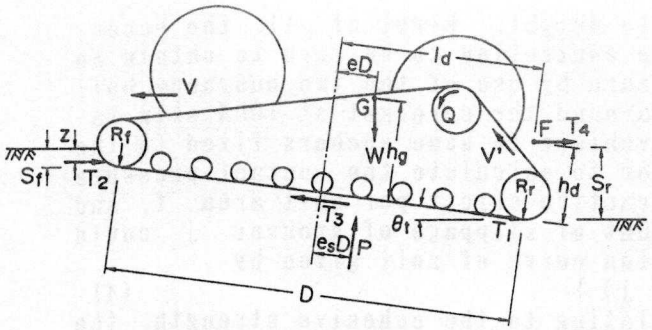

Fig.2 Flexible tracked underwater vehicle ; Dimensions and several forces.

Table 1 Dimensions of underwater vehicle

Weight of vehicle at submerged state	W	44.1 kN
Width of track belt	B	200 cm
Contact length of track belt	D	1000 cm
Mean contact pressure	p_m	1.10 kPa
Radius of frontidler	R_f	60 cm
Radius of rear wheel	R_r	60 cm
Height of grouser	H	4.5 cm
Grouser pitch	G_p	23 cm
Road wheel spacing	R_p	100 cm
Eccentricity	e	0.00
Height of gravity center of vehicle	h_g	250 cm
Distance between central axis of vehicle and point acting drawbar-pull	l_d	500 cm
Height of point acting drawbar-pull	h_d	100 cm
Speed of track belt against vehicle	V'	100 cm/s

of periods.

Fig.2 shows the dimensions of underwater vehicle having two buoyancy tanks to control the contact pressure and the sinkage of track belt. To decrease the locomotion resistance due to an excessive slip sinkage, the contact pressure described in Eq. (2) could be decreased by controlling the vehicle weight W and the eccentricity of gravity center e by use of the right and left buoyancy tanks.

$$p_f = (1-6\,e)\,W\cos\theta_t / 2\,B\,D$$
$$p_r = (1+6\,e)\,W\cos\theta_t / 2\,B\,D \quad (2)$$

where B is the width of track belt and θ_t is the trim angle.

Here, the dimensions of underwater flexible tracked vehicle shown in Table 1 are used to analyze the tractive performance at driving and braking state.

3. Terrain properties

To determine the static sinkage of track belt, the relations between contact pressure p_f, p_r and the corresponding sinkage S_f, S_r should be measured in-situ automatically for various vehicle weight during the settlement of vehicle on the terrain surface. Load cell sensor to measure W, and some sensors to measure S_r and θ_t could be used to decide the static pressure sinkage curve given in Eq.(3).

$$S = b_0\,p^{b_1} \quad (3)$$

The constants b_0 and b_1 are shown in Table 2 for the marine sediment of kaolinite clay[2] self-consolidated under sea water.

To determine the tractive effort, i.e. the thrust or the drag force which is developed on the interface between track belt and marine sediment, the relation between tractive effort, contact pressure and amount of slippage should be

Table 2 Soil properties

Static pressure sinkage	
S<H	b_0 = 25.05
	b_1 = 0.5025
S>H	b_0 = 17.95
	b_1 = 1.45
Shear deformation	
	m_c = 0.139 kPa
	m_f = 0.218
	a = 0.239 1/cm
Slip sinkage	
	c_0 = 0.260
	c_1 = 0.475
	c_2 = 0.854

measured in-situ for various vehicle weight. First of all, the eccentricity of gravity center e should be controlled to be zero to obtain an uniform distribution of contact pressure by use of the two buoyancy balancers. Next, drive the track belt around the sprocket at 100% slip ratio after connecting the underwater vehicle to some anchors fixed to the bottom of the sea. Load cell sensor to calculate the contact pressure p, torque sensor to calculate the tractive effort per unit area f, and rotation sensor to calculate the amount of slippage of grouser j could be used to decide the shear deformation curve of soil given by

$$f = (m_c + m_f \cdot p)\{1 - \exp(-a\,j)\} \tag{4}$$

where m_c, m_f and a are constants relating to the cohesive strength, the angle of internal friction, and the modulus of deformation of soil[3].

Those constants are shown in Table 2 for the same marine sediment.

To determine the slip sinkage of rear wheel given as the summation of each value along the track belt under various contact pressure and amount of slippage, the relation between them should be measured in-situ at the same time. On the same process as the shear deformation curve measurement, the slip sinkage of the grouser takes the same value along the track belt because of the same amount of slippage at any position and it increases with the increment of the travelling time. From the relations between the slip sinkage of track belt S_s and the amount of slippage j i.e. the product of travelling time and the speed of track belt for various contact pressure p, the following equation could be derived as

$$S_s = c_0\, p^{c_1}\, j^{c_2} \tag{5}$$

where c_0, c_1 and c_2 are constants relating to grouser type and shear strength of soil. Also, those constants for the same terrain are shown in Table 2.

4. Simmulation programme

4.1 Tractive effort

As shown in Fig.2, the effective driving or braking force T_4 could be determined from the force balances between driving or braking force T_1, compaction resistance T_2, thrust or drag force T_3, resultant normal force P and W as

$$T_4 = \frac{T_3}{\cos\theta_t} - W \tan\theta_t - T_2 \tag{6}$$

where θ_t is trim angle[4].

4.1.1 Driving state

(a) Thrust

The thrust T_3 could be calculated as the summation of shear resistance which develops on the interface between main straight part of bottom track belt, contact parts of front and rear wheel and terrain.

The thrust T_{mb} acting on the bottom and the 4 side parts of grousers along the main straight part of bottom track belt is calculated as the integration of shear resistance[4),5)].

$$T_{mb} = 2B \int_0^D (m_c + m_f \cdot p)\,[1 - \exp\{-a\,(j_B + i'_d\,X)\}]\,dX + 4H \int_0^D \left\{m_c + m_f \frac{p}{\pi} \cot^{-1}\left(\frac{H}{B}\right)\right\} \cdot [1 - \exp\{-a\,(j_B + i'_d\,X)\}]\,dX \tag{7}$$

$$j_B = (R_f + H)\,[\theta_f - (1 - i_d)\{\sin(\theta_f + \theta_t) - \sin\theta_t\}]$$

$$i'_d = 1 - (1 - i_d)\cos\theta_t$$

$$i_d = 1 - V/V'$$

and θ_f is the entry angle, i_d is the slip ratio, V is the horizontal vehicle speed and V' is the rotation speed of track belt at the top of grousers. The thrusts T_{fd} and T_{rd} developed on the contact parts of front and rear wheel could also be calculated as the integration of shear resistance acting on the bottom and the 4 sides of grousers in the direction of the main straight part of track belt.

Therefore, the thrust T_3 is given by

$$T_3 = T_{md} + T_{fd} + T_{rd} \tag{8}$$

where T_{fd} is zero in the case of the eccentricity e_s larger than 1/6.

(b) Compaction resistance

The vertical sinkage S_r is calculated as the summation of static sinkage given from $b_0(1.2\cdot p_r)^{b_1}\cos\theta_t$ and slip sinkage S_{ri}. The minute slip sinkage ΔS_i during the minute interval d could be given as

$$\Delta S_i = c_0\{p(m\,d)\}^{c_1}[(m\,d)^{c_2} - \{(m-1)\,d\}^{c_2}] \tag{9}$$

$$p(m\,d) = \{p_f + (p_r - p_f)\cdot\left(\frac{m-1/2}{M}\right)\}\{1+\frac{1}{5}\cdot\cos\left(20\,\pi\,\frac{m-1/2}{M}\right)\}$$

$$d = \frac{1}{M}\cdot\frac{i'_d\,D}{1-i'_d} \qquad e_s \leqq \frac{1}{6}$$

Md is the total amount of slippage i.e. the shear deformation of soil on the terrain surface during the passage of vehicle[6].

Then the vertical slip sinkage at rear wheel is given by integrating the above equation as

$$S_{ri} = \left(\sum_{m=1}^{M}\Delta S_i\right)\cdot\cos\theta_t \tag{10}$$

Therefore, T_2 is calculated by

$$T_2 = \frac{2\,b_1\,B}{1+b_1}\left(\frac{1}{b_0}\right)^{1/b_1}\cdot S_r^{(1+b_1)/b_1} \tag{11}$$

(c) Drawbar-pull

Fig.3 shows the flow chart for calculating the traffic performance of flexible tracked vehicle running on the superweak marine sediment. First of all, the initial data : W, B, D, R_f, R_r, p_m, H, e, h_g, l_d, h_d and V'are given. And the soil constants b_0, b_1, m_0, m_f and a and c_0, c_1 and c_2 are read as input data. At rest, p_f, p_r and S_f, S_r, and θ_t are repeatedly calculated until the eccentricity e_{s0} is determined. At slippage state for a given i_d, p_{fi}, p_{ri}, $S_f = S_{f0}$, $S_r = S_{r0} + S_{ri}$, θ_{ti}, T_3, T_2, T_4 are repeatedly calculated until the eccentricity e_{si} is determined. For each slip ratio i_d from zero to 100%, T_1 and T_4 could be calculated by use of a microcomputer and the results are shown in Fig.4.

T_1 decreases gradually with i_d from the maximum value 16.8kN at i_d= 2%.

Also T_4 decreases rapidly with i_d

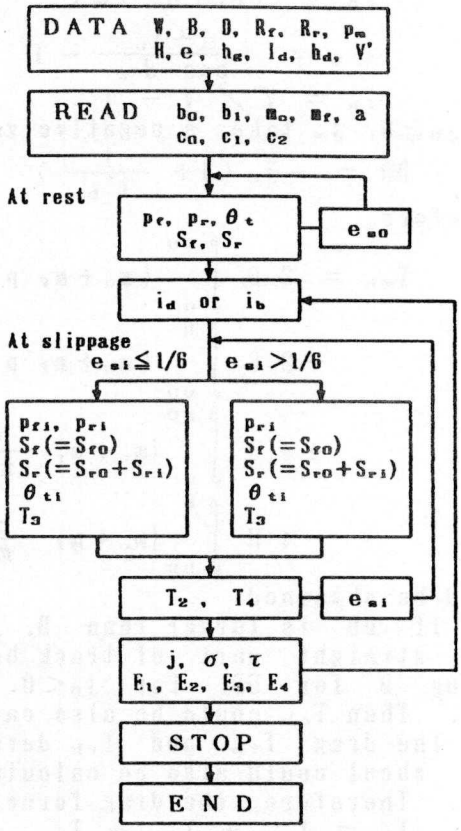

Fig.3 Flow chart

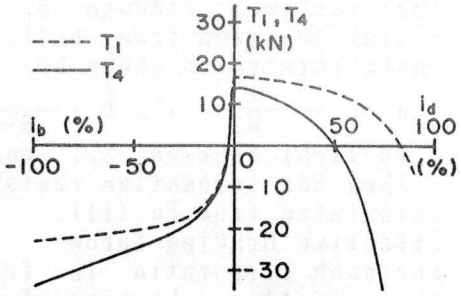

Fig. 4 Relations between driving (or braking) force T_1, drawbar-pull (or effective braking force) T_4 and slip ratio i.

from the maximum one 14.2kN at $i_d = 1\%$ due to the increase of compaction resistance.

4.1.2 Braking state

(a) Drag force

The thrust T_{mb} acting on the bottom and the 4 side parts of grousers along the main straight part of track belt is also calculated for both positive and negative amount of slippage as the integration of shear resistance. The amount of slippage j_m is given by

$$j_m = \frac{i'_b}{1+i'_b} X + j_B \tag{12}$$

$$j_B = (R_r + H)\left[\theta_r - \frac{1}{1+i_b}\{\sin(\theta_r+\theta_t) - \sin\theta_t\}\right]$$

$$i'_b = \frac{1+i_b}{\cos\theta_t} - 1$$

$$i_b = V'/V - 1$$

For $j_B \geqq 0$, j_m takes a negative value from $X = DD$ expressed as

$$DD = -j_B\left(1 + \frac{1}{i'_b}\right) . \tag{13}$$

Therefore,

$$T_{mb} = 2B\int_0^{DD}(m_c + m_r p)\{1-\exp(-a\, j_m)\}\, dX$$

$$-2B\int_{DD}^{D}(m_c + m_r p)\{1-\exp(a\, j_m)\}\, dX$$

$$+4H\int_0^{DD}\{m_c + m_r \frac{p}{\pi}\cot^{-1}\left(\frac{H}{B}\right)\}\{1-\exp(-a\, jm)\}\, dX$$

$$-4H\int_{DD}^{D}\{m_c + m_r \frac{p}{\pi}\cot^{-1}\left(\frac{H}{B}\right)\}\{1-\exp(a\, jm)\}\, dX \tag{14}$$

could be obtained.

If DD is larger than D, j_m takes positive value for all over the main straight part of track belt. T_{mb} could be calculated by substituting D for DD. For $j_B < 0$, j_m takes negative value along the track belt. Then T_{mb} could be also calculated by substituting zero for DD.

The drag T_{fb} and T_{rb} developed on the contact parts of front and rear wheel could also be calculated as the integration of shear resistance. Therefore, the drag force T_3 is given by

$$T_3 = T_{mb} + T_{fb} + T_{rb} \tag{15}$$

where T_{rb} should be zero for the eccentricity e_s larger than 1/6.

(b) Locomotion resistance

The vertical sinkage S_r is also calculated as the summation of static sinkage given from $b_0(1.2p_r)^{b1}\cdot\cos\theta_t$ and slip sinkage S_{ri}. For the minute interval d shown by

$$d = -\frac{1}{M}\cdot i'_b D \cdot \frac{D}{D - j_B(1+i'_b)} \tag{16}$$

, the vertical sinkage S_{ri} could be calculated by use of Eq.(9) and (10). Then the locomotion resistance is given as the compaction resistance calculated from Eq.(11).

(c) Effective braking force

For each slip ratio i_b from zero to -100%, the braking force T_1 and the effective braking T_4 could be calculated by use of the flow chart shown in Fig.3, and the results are shown in the same Fig.4.

T_1 and T_4 decreases rapidly at smaller slip ratio $|i_b|$. Both T_1 and T_4 decreases monotonously at higher slip ratio $|i_b|$, where T_4 is usually smaller than T_1 due to the increasing locomotion resistance.

4.2 Slip sinkage

Fig.5 shows the relations between S_f, S_r and i_d at driving state or i_b at braking state. For both states, S_r is always larger than S_f due to the increasing slip sinkage with slip ratio. On the same slip ratio $i_d = -i_b$, S_r at driving state is comparatively larger than that at braking state due to the difference of amount of slippage.

Fig.6 shows the relation between e_s and i_d or i_b. At driving state, e_s increases rapidly at higher value of slip ratio and reaches 1/6 at $i_d = 90\%$ due to the large amount of slip sinkage S_r. At braking state, e_s increases gradually with the increment of $|i_b|$ and turns from negative value to positive one at $i_b = -56\%$ due to the development of slip sinkage S_r. Fig.6 also shows the relation between θ_t and i_d or i_b. At driving state, θ_t increases parabolically with the increment of i_d. At braking state, θ_t increases almost linearly with $|i_b|$.

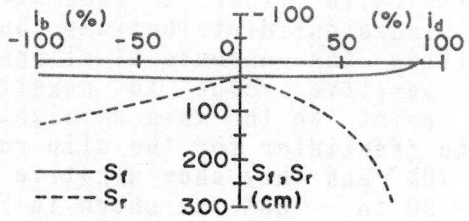

Fig.5 Sinkage of front and rear wheel S_f, S_r and slip ratio i_d, i_b.

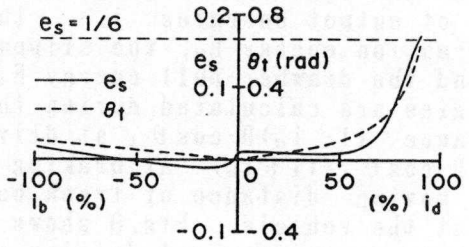

Fig.6 Eccentricity e_s, trim angle θ_t and slip ratio i_d, i_b.

4.3 Stress distribution

At driving state, the amounts of slippage under track belt are positive for the whole range of the contact parts at any slip ratio. The normal stresses σ and shear resistances τ under main straight part of track belt show positive sinusoidal distributions as shown in Fig.7.

At braking state, the amounts of slippage change from positive value to negative one at some point on the main straight part of track belt

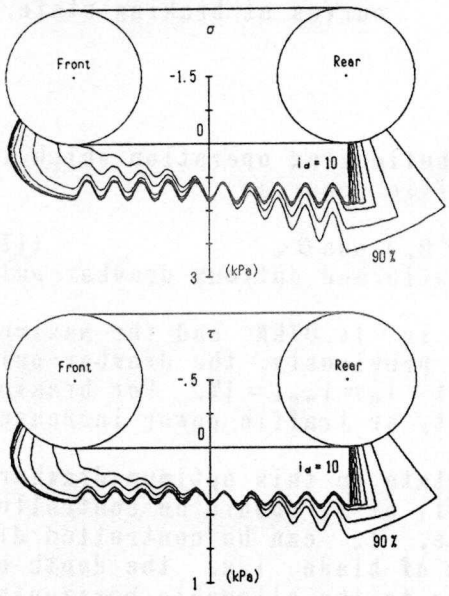

Fig.7 Stress distributions at driving state.

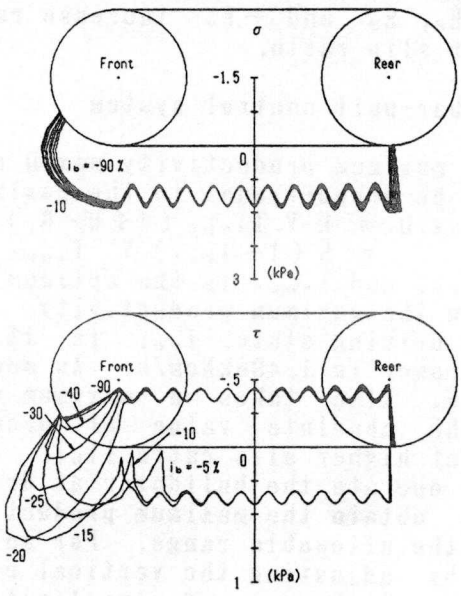

Fig.8 Stress distributions at braking state.

and on the front wheel with the increment of slip ratio $|i_b|$. σ show always positive sinusoidal distributions, but τ with resulting the amounts of slippage change from positive value to negative one at some point on the main straight part and on the frontidler for the slip ratio $i_b = 0$ to -40% and they show negative value for $i_b = -50$ to -100%, as shown in Fig.8.

4.4 Energy balances

The effective input energy E_1 supplied by the sprocket is given by the summation of output energies i.e. the sinkage deformation energy E_2, the slippage energy E_3 and the drawbar-pull energy E_4[4]. Those energies are calculated during the running distance $(1-i_d)D\cdot\cos\theta_t$ at driving state or $D\cdot\cos\theta_t/(1+i_b)$ at braking state for the moving distance of track belt D against the vehicle. Fig.9 shows the energy balance curves at driving state. E_1 decreases parabolically with slip ratio from the maximum value 1.68×10^4 kNcm at $i_d = 3\%$. E_2 increases gradually with slip ratio. E_3 has some maximum value 6.49×10^3 kNcm at $i_d = 56\%$ and reaches to zero at $i_d = 83\%$ where $T_3\cdot\cos\theta_t$ becomes to be $P\cdot\sin\theta_t$. E_4 decreases almost linearly with slip ratio from the peak value 1.50×10^4 kNcm at $i_d = 1\%$ and reaches to zero at $i_d = 50\%$. Fig.10 shows the energy balance curves at braking state. These energies E_1, E_2, E_3 and E_4 develop remarkably in comparison with those energies at driving state. E_2, E_3 and $-E_4$ increase rapidly at higher slip ratio.

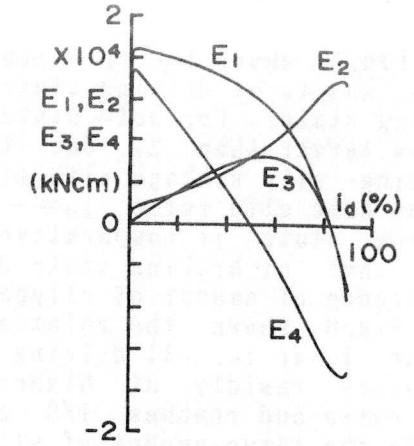

Fig.9 Energy balance curves at driving state.

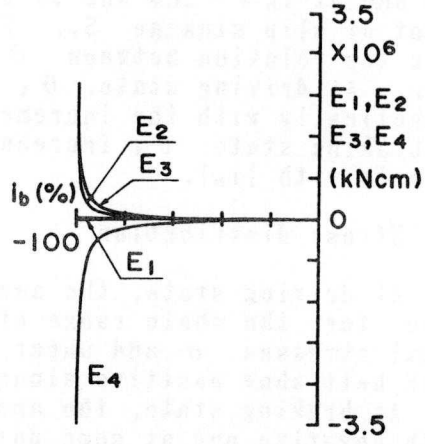

Fig.10 Energy balance curves at braking state.

5. Drawbar-pull control system

The maximum productivity max.Q of the bulldozing operation which is given to be proportional to the maximum traffic power as

$$\max.Q = k\,V\,T_{4opt}\,(1+H/R_r)\cos\theta_t = k\,(1-i_{opt})\,V'\,T_{4opt}\,(1+H/R_r)\cos\theta_t \qquad (17)$$

where i_{opt} and T_{4opt} is the optimum slip ratio and optimum drawbar-pull to obtain the maximum productivity.

For driving state, i_{opt} is 1%, T_{4opt} is 14.07kN and the maximum traffic power is 1.498kNcm/s. As mentioned previously, the drawbar-pull energy E_4 also takes a maximum value at $i_d = i_{opt} = 1\%$. For braking state, the absolute value of productivity or traffic power increases rapidly at higher slip ratio $|i_b|$.

To operate the bulldozer at driving state on this optimum drawbar-pull to obtain the maximum productivity, T_1 or i_d should be controlled within the allowable range. For an example, T_4 can be controlled directly by adjusting the vertical position of blade i.e. the depth of excavation t by use of some limit sensors to the allowable horizontal excavation forces[7] given as

$$T_4 = (1 \pm 0.2)\,T_{4opt} \qquad (18)$$

$$T_{4opt} = 1.8\, R_s\, B'\, t^2\, 10^{-0.45\alpha} \quad (19)$$

where B' is the width of blade, R_s is the specific cutting resistance of soil and α is the rake angle.

6. Conclusion

To obtain the optimum operation of a bulldozer running on a super weak marine sediment, the optimum slip ratio should be determined to obtain the maximum productivity. To develop an automatically drawbar-pull control system, static and slip pressure sinkage curve and shear deformation curve on the interface between terrain and track belt should be determined firstly by use of each sensor. The relations between the driving or braking force, the drawbar-pull or the effective braking force, and slip ratio could be determined rapidly from those terrain properties by use of the microcomputer simmulation programme. Afterwards, the optimum drawbar-pull and the optimum slip ratio could be auto matically determined for the given flexible tracked bulldozer. And the reasonable depth of excavation at the maximum productivity could be controlled by use of a depth sensor.

References

1) D.Rowland : Tracked Vehicle Ground Pressure and its Effect on Soft Ground Performance, Proceedings of the 4th International Conference of ISTVS, Vol.1, pp.353－384, 1972.

2) T.Muro : Grouser Effect on Tractive Performance of a Bulldozer Running on a Superweak Marine Sediment, Proceedings of the 2nd Asia-Pacific Conference of the ISTVS, pp.355－366, 1988.

3) T.Muro : An Optimum Operation of a Bulldozer Running on a Weak Terrain, Proceedings of the 5th International Symposium on Robotics in Construction, JSCE, Vol.2, pp.717－726, 1988.

4) T.Muro, K.Omoto and A.Nagira : Traffic Performance of a Bulldozer Running on a Weak Terrain ――― Energy Analysis ――― , Proc. of JSCE, No.403/VI-10, 1989.

5) M.Shimegi : Designing an Underwater Tractor, Proc. of the Conf. on Off-Highway Vehicle, Tractors and Equipments [GBR], pp.135-142, 1976.

6) T.Muro, K.Omoto and M.Futamura : Traffic Performance of a Bulldozer Running on a Weak Terrain ――― Vehicle Model Test ――― , Proc. of JSCE, No.397/VI-9, pp.151－157, 1988.

7) S.Hata : Construction Machinery, Kajima Press, pp.151－168, 1987.